LUMINESCENCE IMAGING VERSUS LOCK-IN THERMOGRAPHY ON SOLAR CELLS AND WAFERS

Otwin Breitenstein[1], Jan Bauer[1], Karsten Bothe[2], David Hinken[2], Jens Müller[2],
Wolfram Kwapil[3], Martin C. Schubert[4], and Wilhelm Warta[4]
[1]Max Planck Institute of Microstructure Physics, Weinberg 2, D-06120 Halle, Germany
[2]Institute of Solar Energy Research Hamelin (ISFH), Am Ohrberg 1, D-31860 Emmerthal, Germany
[3]FMF, University of Freiburg, Stefan-Meier-Str. 21, D-79104 Freiburg, Germany
[4]Fraunhofer ISE, Heidenhofstraße 2, D-79110 Freiburg, Germany

ABSTRACT: The purpose of this work is a detailed comparison of selected luminescence and lock-in thermography (LIT) results on one exemplary sample and to draw corresponding conclusions. Our focus is on solar cells, but also some investigations on wafers will be discussed. The comparison will help to decide which characterization tools are needed to solve technological problems. It will be demonstrated that luminescence imaging may widely replace LIT with respect to the analysis of recombination-active bulk defects, cracks, series resistances, and junction breakdown sites. However, some important investigations can be done only by LIT. LIT allows for a quantitative analysis of different kinds of leakage currents both under forward and under reverse bias enabling a reliable analysis of local *IV* characteristics. It is shown that LIT and luminescence imaging are complementary to each other and should be used in combination.
Keywords: Characterization, Multi-Crystalline, Shunts, Photoluminescence, Electroluminescence, Lock-in thermography,

1 INTRODUCTION

The technique of infrared (IR) camera-based lock-in thermography (LIT) was described for the first time by Kuo et al. in 1988 [1]. Since 1994 it has been used in solar cell research, first as the "Dynamic Precision Contact Thermography" [2] and later also based on IR-cameras [3]. Meanwhile this technique has been further developed and established as a successful characterization technique for solar cells and other electronic devices [4]. Since 2006 camera-based photoluminescence (PL) imaging [5] and since 2005 electroluminescence (EL) imaging [6] are increasingly used for the local characterization of solar materials and solar cells. Since this luminescence imaging is usually based on a Si-detector camera, it is less expensive then LIT, it does not suffer from thermal blurring, and it usually needs a lower acquisition time than LIT. Meanwhile also for luminescence imaging various techniques have been developed for special imaging tasks. Therefore the question arises: Do we need LIT anymore? In this article first the experimental possibilities of LIT and luminescence imaging are briefly reviewed. Then various variants of both techniques are applied to one exemplary industrial mc-Si solar cell with different imaging tasks. The results show how appropriate both techniques are for evaluating different technological problems (see also [7]).

2 EXPERIMENTAL BASICS

2.1 Lock-in thermography

The dark current-voltage (*IV*) characteristic of a solar cell strongly affects its efficiency, since (together with the short circuit current) it governs the open circuit voltage and the fill factor. Dark lock-in thermography (DLIT) locally images the dissipated power density, which is the product of the local voltage times the local current density. Hence, if series resistance losses are negligible, DLIT directly and quantitatively images the local dark current density. At low forward bias preferentially ohmic shunts and defects leading to the depletion region recombination current (described by the parameter J_{02} of the two-diode model) are imaged, whereas at high forward bias preferentially defects lying in the base and affecting the diffusion current (described by J_{01}) are imaged [4]. It has been found that dark *IV* characteristics are widely governed by local defects, hence most characteristics can only be interpreted based on local analysis [8, 9]. If DLIT is performed at various voltages, local *IV* characteristics can be measured non-destructively [10]. By plane-integrating the DLIT signal over certain regions, also *IV* characteristics of these regions can be obtained, which enable the simulation of the efficiency of these regions treating them as electrically separated from the rest of the cell [11]. By evaluating DLIT images taken at two applied voltages, images of the effective ideality factor and of the saturation current density J_0 can be obtained [11]. If DLIT is performed under reverse bias, breakdown sites are detected, their current can be measured quantitatively, and important breakdown parameters like the slope of the characteristics or the temperature coefficient can be imaged [12, 13]. If LIT is performed at reverse bias under illumination (ILIT), images of the local value of the avalanche multiplication factor may be obtained, enabling the identification of the avalanche breakdown type [13]. Other ILIT techniques image the local monochromatic efficiency including all electrical losses quantitatively [14] or the local series resistance qualitatively [15]. A general limitation of LIT is the degraded spatial resolution caused by thermal blurring. This effect can be reduced by operating at high lock-in frequencies, or it can be corrected by spatial deconvolution [16]. As a drawback, in both cases the sensitivity decreases. If applied to bare wafers, LIT can also be used for spatially resolved measurements of the lifetime in semiconductor wafers by the so-called Infrared Lifetime Mapping (ILM, [17]) or Carrier Density Imaging (CDI [18]), see also [4, 19]. By using these methods under low level injection also trapping centers can be imaged. The spatial resolution of the ILM/CDI method strongly depends on the surface scattering conditions, therefore quantitative results depend on the degree of surface roughness, but also

absolute lifetime measurements are possible, e.g. by Dynamic ILM [20]. Some metals like Fe and Cr tend to yield pairs with boron which may dissociate thermally. If the lifetime before and after thermal treatment is imaged (which can be done also by PL), Fe of Cr imaging can be performed [21, 22].

2.2 Luminescence imaging

There are two variants of luminescence imaging, which are photoluminescence (PL) and electroluminescence (EL). While EL imaging can be applied only on complete solar cells, PL imaging can be performed both on wafers and on cells, where current extraction leads to an additional experimental parameter. Both PL and EL are based on the fact that the radiative recombination rate is proportional to the product of electron and hole concentration with the proportionality factor being a material constant. Thus, the luminescence intensity depends exponentially on the energy separation of the electron- and hole-Fermi level in the bulk. This separation is governed by the local lifetime and, in solar cells, by the local series resistance. Therefore the basic output of luminescence imaging is the local lifetime distribution [5] or the (effective) diffusion length [6]. The amount of light leaving the surface is strongly dependent on the optical surface conditions (roughness). Therefore, for absolute lifetime scaling of luminescence results, they have to be related to other techniques, e.g. [20, 23, 24], or measured dynamically [25]. Moreover, the local distribution of gap states can be imaged by sub-bandgap defect luminescence imaging [26, 27, 28]. For detecting this sub-band-gap emission, an InGaAs IR camera is needed whereas the other luminescence investigations are usually done with a Si-detector camera. On the one hand, a Si-detector camera has a lower quantum efficiency in the wavelength range of the dominant emission in Si (0.9 - 1.1 µm) than an InGaAs camera, hence capturing low-intensity images takes more time. On the other hand, the light detected by a Si-camera shows a certain amount of self-absorption in the Si sample. Therefore, for a Si-based detector, the radiation leaving the sample in a certain position stems mostly from the direct surrounding of this position, whereas for an InGaAs or thermal detector it may be generated several hundred micrometer away, eventually leading to a lower effective spatial resolution depending on the surface roughness. Another reason for the 'smearing' of luminescence images is lateral minority carrier diffusion, which might be overcome by micro-PL in confocal arrangement. However, all these 'smearing' mechanisms of luminescence imaging are less severe than the thermal blurring of LIT. If EL images belonging to two different voltages are evaluated, separate images of the dark series resistance R_s and of the saturation current density J_0 may be obtained. However, this evaluation requires a free fitting parameter [29, 30]. The dark series resistance can also be measured quantitatively by a combination of EL and DLIT (RESI, [31]). With respect to recombination effects EL and PL images show the same lateral distribution. The advantage of PL (without current extraction) over EL is that series resistance effects are negligible as a consequence of homogenous carrier generation. If PL imaging with current extraction is applied to solar cells, images of R_s and J_0 may be obtained independently without any parameter fitting [32, 33]. Until now, here a diode ideality factor of 1 is assumed, and ohmic shunts may disturb this evaluation. If more than three PL images taken under different current extraction conditions are evaluated, the series resistance can be obtained independent of the local diode characteristic [34]. Since the luminescence signal reacts very sensitively to tiny variations of the local voltage, luminescence-based R_s imaging is very sensitive and easily detects e.g. broken contact fingers. Moreover, in luminescence images cracks and also stronger ohmic shunts are visible [35]. Quantitative shunt measurements are possible [36] but not as straightforward as for DLIT. Weak ohmic shunts may remain invisible if they are lying below a grid line. Also defects being responsible for the depletion region recombination current J_{02} remain invisible in luminescence imaging as long as they do not seriously affect the local voltage. Note that in the bulk the depletion region recombination current is a majority carrier current. Recently also ideality factor imaging by PL has been proposed, but this technique shows a poor spatial resolution and works only for cells without grid [37]. EL imaging performed under reverse bias is called ReBEL (Reverse Bias EL [38]). The use of another name is justified here since ReBEL relies on completely different physical processes than forward bias EL and shows a very different spectrum [39]. Though also ReBEL may measure *IV* characteristics of breakdown sites [26], the proportionality factor depends on the breakdown type, and strong ohmic shunts show no ReBEL light emission at all. By evaluating ReBEL data for various voltages images of the local breakdown voltage may be obtained [40].

3 WAFER INSPECTION

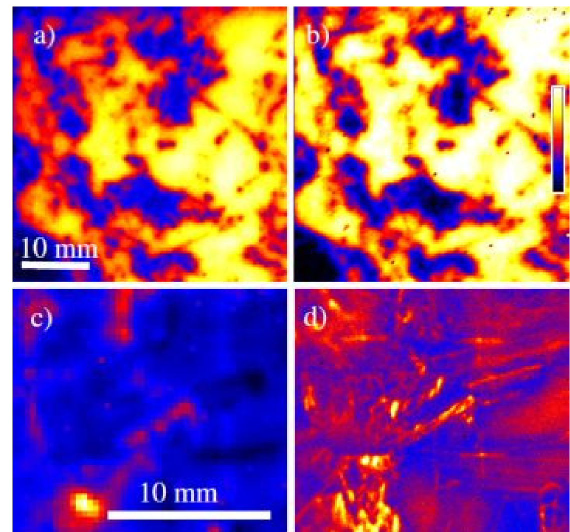

Figure 1: a) Lifetime image of sample A measured by PL with Si camera, b) lifetime image of the same region measured by CDI (both images scaled from 0 to 180 µs [5]), c) defect luminescence image of sample B (measured in spot scanning mode), d) CDI/ILM trap density image of the same region (both images given in a.u. [27])

Lifetime images of crystalline silicon wafers may be obtained both by PL [5] and by CDI/ILM imaging [17, 18, 19]. Thus, the imaging of the iron or chromium concentration in wafers, based on lifetime images taken before and after Fe/Cr-B-pair dissociation, is possible both by PL and CDI/ILM [21, 22]. For PL on crystalline

silicon wafers and cells, usually a silicon-based detector is used. The better spatial resolution obtained by this detector is the main reason why PL lifetime images may show a slightly better spatial resolution than CDI/ILM images. This is demonstrated in Fig. 1 a) and b), taken from [5], where some more details are visible in a) than in b). CDI/ILM may also detect trapping centers, which is impossible by PL/EL, but only PL/EL may detect defect luminescence, if an InGaAs camera and appropriate optical filtering is used. An example of a comparison between the trap density and the defect luminescence (here gained by photoluminescence spectroscopy mapping) on another sample is shown in Fig. 1 c) and d) [27], demonstrating that the defect state and the trapping center distribution correlate but are not identical. Generally, except for investigating trapping centers, PL is preferred today to CDI/ILM for lifetime imaging on wafers.

4 SOLAR CELL INVESTIGATIONS

Most results in this section were obtained on one and the same multicrystalline "standard" solar cell. It is a 156x156 mm^2 acidic textured industrial multicrystalline silicon solar cell with a full-area Al-alloyed back contact having an energy conversion efficiency of 15.2 %.

4.1 Bulk defect imaging

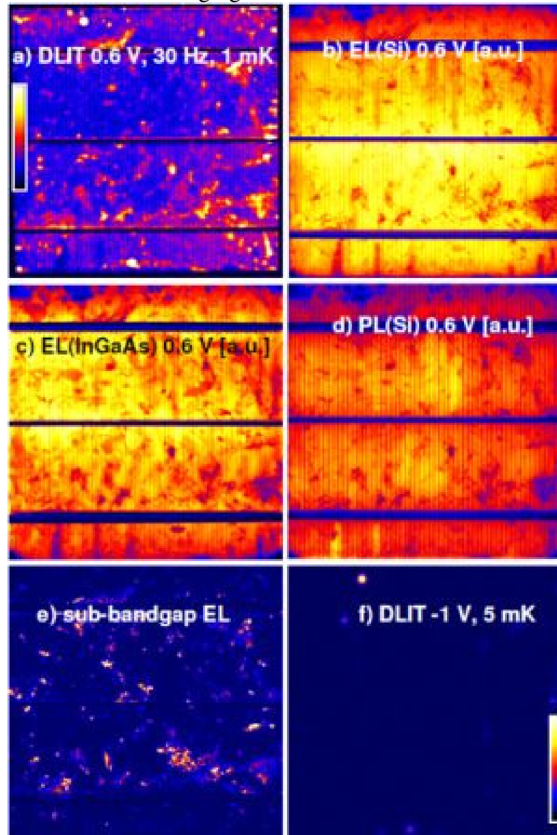

Figure 2: a) DLIT amplitude image at 0.6 V, b) EL image (Si camera) at 0.6 V [a.u.], c) EL image (InGaAs camera) at 0.6 V [a.u.], d) PL image (Si camera) at 0.6 V with current extraction, e) Forward bias defect luminescence EL image of the cell (0.6V, 3A) [a.u.], f) DLIT image at -1 V showing only ohmic shunts (amplitude image, 10 Hz, scaled to 5 mK)

Recombination-active defects in the bulk of solar cells can be imaged both by luminescence imaging (usually EL, which is easier than PL) and dark lock-in thermography (DLIT). Here DLIT at high voltages close to V_{oc} should be used, where the diffusion current dominates, which depends on the bulk lifetime. In defect regions with low lifetime the DLIT signal is higher. Fig. 2 shows such a comparison for the standard cell. Even though the DLIT image (Fig. 2 a) is measured at a relatively high frequency of 30 Hz, it clearly shows a degraded spatial resolution compared to EL (Fig. 2 b) due to the inevitable thermal blurring. While the acquisition time for image a) was 1 hr, less than 1 minute was necessary for image b). Thus, for bulk defect imaging EL is clearly superior. The EL image also shows series resistance effects which will be discussed later on. However at the top edge it shows a number of very dark spots of unknown origin which are not reflected in the DLIT image. Most probably these dark spots are caused by defect or impurity clusters since they are also found on neighboring cells. Note that this upper cell edge was close to the crucible wall during crystallization. Fig. 2 c) shows an EL image also taken at 0.6 V by using an InGaAs camera. Here the acquisition time was only in the order of seconds. However, due to the lower self-absorption the spatial resolution of c) is clearly degraded compared to b). Fig. 2 d) shows a PL image of this cell, again imaged at 0.6 V with a Si camera, where some current was extracted (note that V_{oc} of this cell was above 0.6 V). Here the regions of increased series resistance (broken grid fingers), which appeared dark in (b), appear brighter, since the local voltage is higher there. This is the physical effect underlying PL-based series resistance imaging. Finally Fig. 2 e) shows a defect luminescence EL image of this cell taken with an InGaAs camera by filtering out the bandgap luminescence.

4.2 Ohmic shunt imaging

Most of the defects visible in Fig. 2 a) show a non-linear (diode-like) *IV*-characteristic, hence they may be called "non-linear shunts". In most cases these defects are recombination-induced, whereas ohmic shunts may originate from Al-particles, insufficient edge opening, or SiC filaments [41]. In DLIT ohmic shunts can easily be identified by applying a weak reverse bias where only ohmic shunts contribute to the image. The DLIT image of the standard cell in Fig. 2 f) taken at -1 V (-21 mA flowing) shows that only a few of the shunts are ohmic. In EL images these ohmic shunts may appear as weak dark spots. Hence, in EL/PL weak ohmic shunts can hardly be distinguished from recombination-active defects. If they are located below grid lines, they are generally invisible in EL. Stronger ohmic shunts can be seen in a luminescence image as blurred dark regions with a spatial resolution worse than in DLIT [35]. Thus, for ohmic shunt imaging and identification, DLIT is clearly superior to EL/PL imaging.

4.3 Crack imaging

Fig. 3 shows a monocrystalline cell containing cracks. Here the DLIT image a) is a 0°-image taken at 10 Hz, which shows a better spatial resolution than the DLIT amplitude image. Nevertheless, the spatial resolution of the EL image b) is better (only EL can identify that some of the cracks are two parallel lying cracks), and the acquisition time for EL was significantly lower. Therefore, for crack detection EL imaging is preferred. In

multicrystalline material it may be difficult for both techniques to distinguish cracks from grain boundaries and other defects. This problem has recently been treated by Demant et al. [42] by applying a dedicated image processing algorithm.

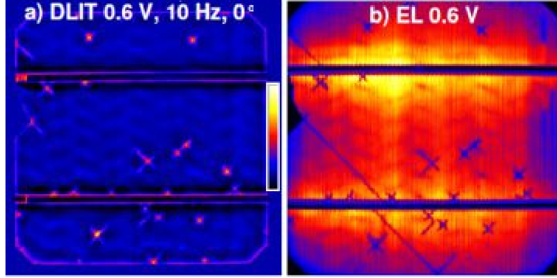

Figure 3: a) DLIT (0° image, scaled to 10 mK), b) EL image [a.u.] of a cracked monocrystalline cell

4.4 Series resistance imaging

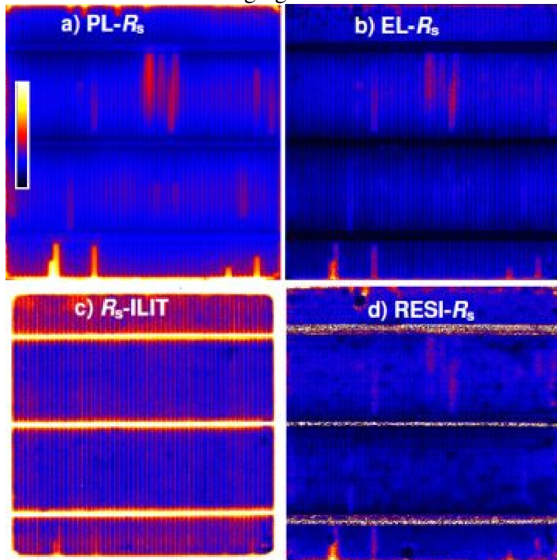

Fig. 4: a) PL-R_s image after Trupke [32], scaled from 0 to 3 Ωcm^2, b) EL-R_s image [30] in a.u., c) R_s-ILIT image [15] in a.u., d) RESI-R_s image [31], scaled from 0 to 3 Ωcm^2

The local area-related series resistance $R_s(x,y)$ in solar cells (given in units of Ωcm^2) is defined as the local voltage drop between terminals and the local diode, divided by the locally flowing current density. One has to distinguish between light (illuminated) and dark series resistance, since in the high current regime the current paths are different. In Fig. 4 various series resistance images of the standard cell already used for Fig. 2 are shown. We see that the PL-R_s image after Trupke [32] (Fig. 4 a) does not show any artifacts due to local recombination centers or other current sinks. On our sample, the more complicated procedure after Kampwerth [34] does not give significantly better results. In EL-R_s (Fig. 4 b) [30] some dark spots are visible at the top edge, which may be an artifact coming from the Fuyuki-approximation [6, 29]. R_s-ILIT (Fig. 4 c) (which was shunt-corrected here, see [15]) is less sensitive than luminescence and may image only the strongest R_s-variations. Note that in the dark R_s image d) obtained by RESI [31] the local shunts (see bright spots in Fig. 2 a) appear as regions with low series resistance (black spots on blue background in Fig. 4 d). This is due to the fact that the currently used concept of area-related series resistance actually assumes homogeneous current flow, which is better realized under illumination than in the dark. We find that luminescence imaging (esp. PL with current extraction) leads to the most sensitive and reliable R_s images.

4.5 Local *IV* characteristics analysis

The big advantage of LIT is that it directly images the locally dissipated power density $p(x,y)$. Thus, if the series resistance is negligible, the DLIT signal $T(x,y)$ in a certain position can be measured as a function of applied bias V. Then the local *IV* characteristic may be measured non-destructively (up to an unknown factor) by plotting $T(x,y)/V$ versus V [10]. Assume that the whole cell is imaged, the IR emissivity is sufficiently homogeneous, and the total power P dissipated by the whole cell with area A is known. Then, within the spatial resolution limit of the thermal diffusion length (typically 1-2 mm), $p(x,y)$ may be calculated from the local -90° signal $T^{-90°}(x,y)$ by [4]

$$p(x,y) = \frac{P\,T^{-90°}(x,y)}{A < T^{-90°}(x,y) >} . \qquad (1)$$

Here $<T^{-90°}(x,y)>$ is the thermal signal averaged over the whole cell. Eq. (1) is the basis of several techniques for quantitative evaluation of LIT images [4, 11, 12, 43].

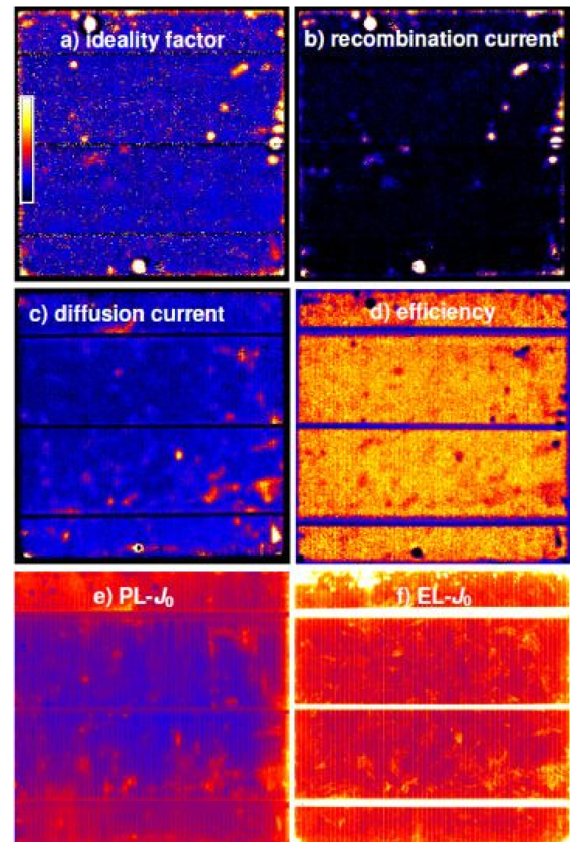

Figure 5: a) Effective ideality factor, scaled from 0 to 5 [11], b) recombination current density at 0.55 V and c) diffusion current density at 0.55V, both scaled from 0 to 10^{-2} A/cm^2 [43], d) monochromatic (850 nm) efficiency [14], scaled from -10 % to +44 %, e) PL-J_0 image (0 to 2.5×10^{-12} A/cm^2 [33]), f) EL-J_0 image (a.u.) [30]

For example, Fig. 5 a) shows the ideality factor image of the standard cell measured between 0.525 and 0.55 V [11]. Note that this is the effective ideality factor n_{eff} holding for the whole diode current and not only for the recombination current contribution. In most of the area n_{eff} is close to 1, but in the edge region and in some defect positions it increases up to 5 and above (see [8]). The large values at the positions of ohmic shunts (see Fig. 2 f) are artifacts of the evaluation which assumes an exponential dependence. Fig. 5 b) and c) show the separation of the current density at 0.55 V into the (depletion region) recombination current b) and the diffusion current density c) according to [43]. In most of the area, both in regions of good and of poor crystal quality, the current at 0.55 V is mostly a diffusion current, as the effective ideality factor image a) already has suggested. Near the edges and in some specific positions, where the ideality factor is large, the dominating current is a depletion region recombination current. Thus, by comparing Figs. 5 b) and c), non-linear shunts caused by depletion region recombination and bulk recombination may be distinguished from each other.

The monochromatic efficiency at 850 nm at the working point is displayed in Fig. 5 d). This ILIT-based image is based on the fact that, in regions where electric power is generated, the thermal heating is reduced [14]. Negative values of the efficiency in shunt positions indicate that power is consumed there. By comparison with Fig. 4 we see that the regions of increased series resistance do not significantly affect the locally generated power. Finally, Fig. 5 e) and f) show J_0 images obtained from PL [33] and EL evaluations [30], respectively. These have to be compared with Fig. 5 c) and Fig. 2 a), which is also dominated by J_{01}. Even though the images are differently scaled, some significant differences can be observed. The spatial resolution is considerably better in the luminescence images, but both luminescence images differ from each other, and the image contrast (highest signal vs. homogeneous background signal) is significantly lower in the EL/PL-based images. The reason for these discrepancies is not clear yet. The DLIT results can be expected to be more realistic, since they are measured more directly.

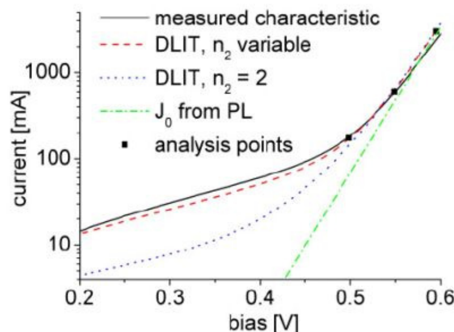

Figure 6: Measured global IV characteristic of the cell investigated here compared to characteristics simulated from DLIT analysis (assuming variable and fixed ideality factor n_2) and from PL analysis

As a validity check for the various methods for imaging the local dark characteristics, the local currents of all image positions may be summed up to yield the global characteristic, which may be compared with the measured one. The result for our sample is shown in Fig. 6, which shows the measured characteristic together with some simulated ones. Note that the measured characteristic contains the influence of the series resistance, but the simulated characteristics do not. The three dots are the averaged current vs. local voltage data of the cell during the three forward bias DLIT measurements, also without considering the series resistance. The best correspondence is obtained with the Local I-V procedure after [43] based on the data used for Figs. 2 f), 5 b) and 5 c), assuming a variable ideality factor of the recombination current n_2. Very often this ideality factor is set to two. This assumption leads to a degraded fit for lower voltages, here the lowest voltage analysis point is badly fitted. If an ideality factor of 1 is assumed for the characteristic, as done until now for all PL and EL evaluation methods, the data of Fig. 5 e) allow to fit only the highest voltage measurement point at 0.6 V, but the low voltage part strongly deviates from the measured characteristic. Altogether, it can be concluded that, for local *IV* characteristic analysis, LIT investigations are more reliable than luminescence techniques.

4.6 Breakdown imaging

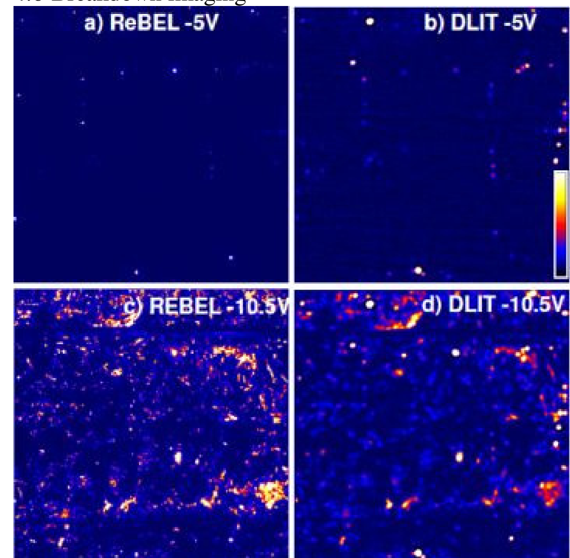

Figure 7: a) ReBEL at -5 V, b) DLIT at -5 V, c) ReBEL at -10.5 V, d) DLIT at -10.5 V

Theoretically, a solar cell with a base doping concentration of 10^{16} cm^{-3} should breakdown beyond -50 V reverse bias [44]. In reality, in multicrystalline cells non-linear breakdown starts already at a few V reverse bias [12]. This "pre-breakdown" phenomenon can be investigated both by DLIT and by reverse-bias EL (ReBEL) [12, 26, 38]. Here DLIT may be faster than ReBEL, depending on the quality of the camera. Fig. 7 shows a comparison of DLIT and ReBEL images at -5 V and at -10.5 V. The scaling limits are different, but results of each bias may be compared relatively to each other. Again, the spatial resolution of the luminescence images is better than that of the DLIT images. Even though most breakdown sites can be seen in both images, the quantitative correlation is poor at -5V. Some of the sites visible in DLIT even remain completely invisible in ReBEL. This means that early breakdown sites and weak ohmic shunts dominating at -5 V may not be measured reliably by ReBEL. At -10.5 V, where the breakdown current is mainly caused by local imperfections [12], the

correlation is much better. However, also here the strong shunts, which dominate the DLIT images, appear relatively weaker in the ReBEL image. Hence, for qualitative breakdown localization ReBEL is appropriate and shows a clearly better spatial resolution than DLIT, but it does not yield the correct reverse currents at low voltages.

4.7 Breakdown analysis

Fig. 8 shows three LIT-based images [13] and one ReBEL-based image [40] for a detailed analysis of the local breakdown process. In Fig. 8 a) the temperature coefficient (*TC*) at -10.7 V, derived from two images measured at 25 and 40 °C, is displayed. Without going into any details, we see that regions with positive and with negative *TC* can be clearly distinguished. The slope image b) taken at 25°C between -10.5 and -10.7 V shows regions of different (relative) steepness of the breakdown characteristic. Some spots with strongly negative *TC* show a higher slope. The avalanche multiplication factor (*MF*) image c) taken at 25 °C between -10.5 V (no avalanche multiplication) and -10.7 V shows that, in this small bias range, the *MF* increases in some regions to above 10. Finally, in Fig. 8 d) the breakdown voltage has been imaged by evaluating the onset voltage of the local ReBEL signal [40]. The breakdown regions (see Fig. 7) are visible as dark spots. The darker the spot in Fig. 8 d), the lower is the breakdown voltage. The regions of high avalanche *MF* in c) are characterized by a higher breakdown voltage (red spots in Fig. 8 d), whereas the points of early breakdown in Fig. 7 a) show darker spots in Fig. 8 d). This breakdown voltage imaging could also be performed by DLIT, but here the limited spatial resolution would be a limitation. In conclusion, compared to ReBEL, DLIT allows for a more detailed analysis and the extraction of parameters clarifying the physical origin/mechanism of local breakdown sites.

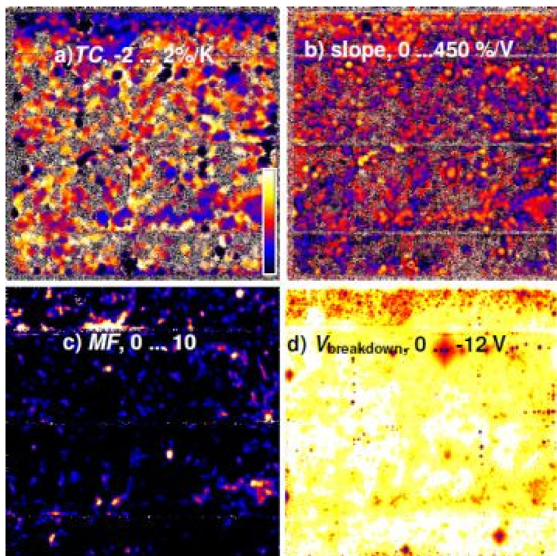

Figure 8: a) Temperature coefficient image, b) slope image, c) multiplication factor image, d) ReBEL-based breakdown voltage image

5 CONCLUSION

The result of this comparison are summarized in a ranking in Tab. 1. Here "++" means "very appropriate", "+" means "appropriate", - means "less appropriate", and "--" means "not appropriate". The total score of LIT is 15 x "+" and 3 x "-", and for EL/PL it is 15 x "+" and 4 x "-". Considering our subjective point of view, this ranking is very balanced. The result is that both LIT- and luminescence-based methods have their own strengths and weaknesses. The appropriate method depends on the specific technological problem to be studied. While EL/PL is superior for lifetime mapping, bulk defect imaging, series resistance imaging and exact junction breakdown site imaging, for all tasks requiring quantitative current measurements LIT-based techniques are superior. Some tasks, like weak ohmic shunt identification and detection of trapping centers, can be performed only by LIT techniques, whereas other tasks, like defect luminescence imaging, can be done only by luminescence. Thus, both techniques should be used in parallel.

Imaging task	**LIT**	**EL/PL**	**Remarks**
lifetime in wafers	+	++	EL/PL better resolution
trapping centers	++	--	ILM/CDI
defect luminescence	--	++	InGaAs camera
metal-boron pairs	+	++	LIT in CDI/ILM mode
bulk defects in cells	+	++	EL/PL better resolution
weak ohmic shunts	++	-	EL not if under gridline
strong ohmic shunts	++	+	EL more blurred
cracks	+	++	EL/PL better resolution
series resistance	-	++	PL most reliable
local IV characteristics	++	-	EL/PL until now only J_{01}
breakdown sites	+	+	ReBEL better resolution DLIT really quantitative
breakdown analysis	++	+	ReBEL better resolution LIT more possibilities

Tab. 1: Scoring of LIT and EL/PL for different imaging tasks

References

[1] P.K. Kuo, T. Ahmed, H. Jin, R.L. Thomas, "Phase-locked image acquisition in thermography", *SPIE* **1004**, 1988, 41-45.

[2] O. Breitenstein, W. Eberhardt, K. Iwig, "Imaging the local forward current density of solar cells by dynamical precision contact thermography", *1st World Conf. on Photovolt. Energy Conversion*, Hawaii 1994, pp. 1633-1636.

[3] O. Breitenstein, M. Langenkamp, O. Lang, and A. Schirrmacher, "Shunts due to laser scribing of solar cells evaluated by highly sensitive lock-in thermography", *Solar Energy Materials and Solar Cells* **65**, 2000, pp. 55-62.

[4] O. Breitenstein, W. Warta, M. Langenkamp, "*Lock-in Thermography - Basics and Use for Evaluating Electronic Devices and Materials*", 2nd edition, Springer (Berlin/Heidelberg) 2010.

[5] T. Trupke, R.A. Bardos, M.C. Schubert, W. Warta, "Photoluminescence imaging of silicon wafers", *Appl. Phys. Lett.* **89**, 2006, 044107.

[6] T. Fuyuki, H. Kondo, T. Yamazaki, Y. Takahashi, Y. Uraoka, "Photographic surveying of minority carrier diffusion length in polycrystalline silicon solar cells by electroluminescence", *Appl. Phys. Lett.* **86**, 2005, 262108.

[7] O. Breitenstein, J. Bauer, K. Bothe, D. Hinken, J. Müller, W. Kwapil, M.C. Schubert, W. Warta, "Can luminescence imaging replace lock-in thermography on solar cells?", contribution at *37th IEEE PVSC*, Seattle 2011, to be published in IEEE J-PV.

[8] S. Steingrube, O. Breitenstein, K. Ramspeck, S. Glunz, A. Schenk, P.P. Altermatt, "Explanation of commonly observed shunt currents in c-Si solar cells by means of recombination statistics beyond the Shockley-Read-Hall approximation", *J. Appl. Phys.* 110, 2011, 014515.

[9] D. Hinken, K. Bothe, R. Brendel, "Impact of lateral variations on the solar cell efficiency", *25th EU PVSEC*, Valencia 2010, pp. 1367-1372.

[10] I.E. Konovalov, O. Breitenstein, and K. Iwig, "Local current-voltage curves measured thermally (LIVT): a new technique of characterizing PV cells", *Solar Energy Materials and Solar Cells* **48**, 1997, pp. 53-60.

[11] O. Breitenstein, J.P. Rakotoniaina, M.H. Al Rifai, "Quantitative Evaluation of Shunts in Solar Cells by Lock-in Thermography", *Prog. Photovolt: Res. Appl.* **11,** 2003, pp. 515-526.

[12] O. Breitenstein, J. Bauer, K. Bothe, W. Kwapil, D. Lausch, U. Rau, J. Schmidt, M. Schneemann, M.C. Schubert, J.-M. Wagner, W. Warta, "Understanding junction breakdown in multicrystalline solar cells", *J. Appl. Phys.* **109**, 2011, 071101.

[13] O. Breitenstein, J. Bauer, J.-M. Wagner, A. Lotnyk, "Imaging physical parameters of pre-breakdown sites by lock-in thermography techniques", *Prog. Photovolt: Res. Appl.* **16,** 2008, pp. 679-685.

[14] K. Ramspeck, K. Bothe, J. Schmidt, R. Brendel, "Correlation between spatially resolved solar cell efficiency and carrier lifetime of multicrystalline silicon", *J. Mat. Sci: Mater. Electron.* **19**, 2008, pp. S4-S8.

[15] O. Breitenstein, J.P. Rakotoniaina, A.S.H. van der Heide, J. Carstensen, "Series Resistance Imaging in Solar Cells by Lock-in Thermography", *Prog. Photovolt: Res. Appl.* **13**, 2005, pp. 645-660.

[16] I. Konovalov and O. Breitenstein, "Evaluation of Thermographic Investigations of Solar Cells by Spatial Deconvolution", *2nd World Conference on Photovoltaic Energy Conversion*, Wien 1998, pp. 148-151.

[17] M.Bail, J. Kentsch, R. Brendel and M. Schulz, "Lifetime mapping of Si wafers by an infrared camera", *28th IEEE-PVSC*, Anchorage 2000, pp. 99-103.

[18] S. Riepe, J. Isenberg, C. Ballif, S.W. Glunz and W. Warta, "Carrier density imaging and lifetime imaging of silicon wafers by infrared lock-in thermography", Proc. *17th EU-PVSEC*, Munich 2001, pp. 1597 – 1599.

[19] W. Warta, "Advanced Defect and Impurity Diagnostics in Silicon Based on Carrier Lifetime Measurements", *Phys. Stat. Sol. (a)* **203**, 2006, pp. 732-746.

[20] K. Ramspeck, S. Reissenweber, J. Schmidt, K. Bothe, R. Brendel, "Dynamic carrier lifetime imaging of silicon wafers using an infrared-camera-based approach", *Appl. Phys. Lett.* **93**, 2008, 102104

[21] D. Macdonald, J. Tan, T. Trupke, "Imaging interstitial iron concentration in boron-doped crystalline silicon using photoluminescence". *J. Appl. Phys.* **103**, 2008, 73710.

[22] H. Habenicht, M.C. Schubert, W. Warta, "Imaging of chromium point defects in p-type silicon", *J. Appl. Phys.* **108**, 2010, 034909.

[23] S. Herlufsen, J. Schmidt, D. Hinken, K. Bothe, R. Brendel, "Photoconductance-calibrated photoluminescence lifetime imaging of crystalline silicon", *Phys. Stat. Sol. (RRL)* **2**, 2008, pp. 245-247.

[24] J. A. Giesecke, M. C. Schubert, B. Michl, F. Schindler, and W. Warta, "Minority carrier lifetime imaging of silicon wafers calibrated by quasi-steady-state photoluminescence", *Solar Energy Materials & Solar Cells* **95**, 2011, pp. 1011-1018.

[25] S. Herlufsen, K. Ramspeck, D. Hinken, A. Schmidt, J. Müller, K. Bothe, J. Schmidt, R. Brendel, "Dynamic photoluminescence lifetime imaging for the characterization of silicon wafers", *Phys. Stat. Sol. (RRL)* **5**, 2011, pp. 25–27.

[26] K. Bothe, D. Hinken, K. Ramspeck, S. Herlufsen, J. Schmidt, R. Brendel, J. Bauer, J.-M. Wagner, N. Zakharov, O. Breitenstein, "Imaging and Analysis of Pre-Breakdown Sites in Multicrystalline Silicon Solar Cells", *24th EU PVSEC*, Hamburg 2009, pp. 918-924.

[27] M.C. Schubert, P. Gundel, M. The, W. Warta, "Spatially resolved luminescence spectroscopy on multicrystalline silicon", *23th EU PVSEC*, Valencia 2008, pp. 17-23.

[28] M. Kasemann, W. Kwapil, M. C. Schubert, H. Habenicht, B. Walter, M. The, S. Kontermann, S. Rein, O. Breitenstein, J. Bauer, A. Lotnyk, B. Michl, H. Nagel, A. Schütt, J. Carstensen, H. Föll, T. Trupke, Y. Augarten, H. Kampwerth, R. A. Bardos, S. Pingel, J. Berghold, W. Warta, and S. W. Glunz, "Spatially resolved silicon solar cell characterization using infrared imaging methods", 3*3rd IEEE PVSC*, San Diego 2008.

[29] J. Haunschild, M. Glatthaar, M. Kasemann, S. Rein, E.R. Weber, "Fast series resistance imaging for silicon solar cells using electroluminescence", *Phys. Stat. Sol. RRL* **3**, 2009, pp. 227-229.

[30] O. Breitenstein, A. Khanna, Y. Augarten, J. Bauer, J.-M. Wagner, K. Iwig, "Quantitative evaluation of electroluminescence images of solar cells", *Phys. Stat. Sol. RRL* **4**, 2010, pp. 7-9.

[31] K. Ramspeck, K. Bothe, D. Hinken, B. Fischer, J. Schmidt, R. Brendel, "Recombination current and series resistance imaging of solar cells by combined luminescence and lock-in thermography", *Appl. Phys. Lett*, **90**, 2007, 153502.

[32] T. Trupke, E. Pink, R. A. Bardos, M. D. Abbott, "Spatially resolved series resistance of silicon solar cells obtained from luminescence imaging", *Appl. Phys. Lett.* **90**, 2007, 093506.

[33] M. Glatthaar, J. Haunschild, M. Kasemann, J. Giesecke, W. Warta, "Spatially resolved determination of dark saturation current and series resistance of silicon solar cells", *Phys. Stat. Sol. RRL* **4**, 2010, pp. 13-15.

[34] H. Kampwerth, T. Trupke, J.W. Weber, Y. Augarten, "Advanced luminescence based effective series resistance imaging of silicon solar cells", *Appl. Phys. Lett.* **93**, 2008, 202102.

[35] O. Breitenstein, J. Bauer, T. Trupke, R.A. Bardos, "On the detection of shunts in silicon solar cells by photo- and electroluminescence imaging", *Prog. Photovolt: Res. Appl.* **16**, 2008, pp. 325-330.

[36] Y. Augarten, T. Trupke, M. Lenio, J. Bauer, O. Breitenstein, J. Weber, R.A. Bardos, "Luminescence shunt imaging: Qualitative and quantitative shunt images using photoluminescence imaging", *25th EU PVSEC*, Hamburg 2009, pp. 29-32.

[37] L. Stoicescu, G.C. Glaeser, M. Reuter, U. Rau, J.H. Werner, "Ideality factor extraction from photoluminescence images", Proc. 25th EU PVSEC, Valencia 2010, pp. 24-28.

[38] D. Lausch, K. Petter, H. v. Wenckstern, M. Grundmann, "Correlation of pre-breakdown sites and bulk defects in multicrystalline silicon solar cells", *Phys. Stat. Sol. RRL* **3**, 2009, pp.70-72.

[39] M. Schneemann, Th. Kircharz, R. Carius, U. Rau, A. Helbig, "Spatially resolved reverse biased electroluminescence spectroscopy of crystalline silicon solar cells", *25th EU PVSEC*, Valencia 2010, pp. 24-28.

[40] W. Kwapil et al., "Diode breakdown related to recombination active defects in block-cast multicrystalline silicon solar cells", *J. Appl. Phys.* **106**, 2009, 063530.

[41] O. Breitenstein, J.P. Rakotoniaina, H.H. Al Rifai, M. Werner, "Shunt types in crystalline silicon solar cells", *Prog. Photovolt: Res. Appl.* **12**, 2004, pp. 529-538.

[42] M. Demant, S. Rein, J. Krisch, S. Schoenfelder, C. Fischer, S. Bartsch, R. Preu, "Detection and analysis of micro-cracks in multi-crystalline silicon wafers during solar cell production", contribution at *37th IEEE PVSC*, Seattle 2011, in print.

[43] O. Breitenstein, "Nondestructive local analysis of current-voltage characteristics of solar cells by lock-in thermography", *Solar Energy Mat. & Solar Cells* **95**, 2011, pp. 2933-2936.

[44] S.M. Sze, G. Gibbons, "Effect of junction curvature on breakdown voltage in semicconductors", *Solid-State Electron.* 9, 1966, pp. 831-845.